Did you forget the measurement uncertainty doing your connectivity analysis?

Martin Stigsson

SKB, Swedish Nuclear Fuel and Waste Management Co,
Solna, Sweden

KTH, Royal Institute of Technology, Sustainable Development, Environmental Science and Engineering (SEED),
Stockholm, Sweden

ABSTRACT: Many engineering applications in crystalline rocks use fracture intercepts mapped in boreholes as foundation. From this mapping the distributions of intensity, spatiality and orientation can be inferred. These three distributions combined with the size distribution steer the connectivity of the fracture network and hence the nature of groundwater flow and transport of solutes. This study, however, only focuses on the impact that the orientation uncertainty has on the connectivity. The orientation of a fracture intersecting a borehole can be calculated using four angles, each afflicted with uncertainty. These uncertainties are used to distinguish between natural variability and uncertainty using a χ^2 test of a contingency table of fracture poles. Two DFN models are developed, the rock mass fracture and the "measured" model, and the differences in connectivity between the models are analyzed. The rock mass fracture model have 30% more connected fractures, 60% more connected fracture area and is more elongated than the "measured" model at the connectivity level when the first fracture of the two clusters hits any boundary of the modelling cube.

1. INTRODUCTION

Many engineering applications in crystalline rocks use fracture intercepts mapped in boreholes as foundation. From the mapping in the boreholes, the distributions of intensity, spatiality and orientation can be inferred. These three parameter distributions in combination with the size distribution steer the connectivity of the fracture network and hence the nature of groundwater flow and transport of solutes.

Commonly, only the expected orientations of mapped fractures are inferred whilst the uncertainty in the inference is generally neglected. Stigsson, 2016, showed that neglecting the uncertainty may impact the inference of fracture orientation distribution parameters as well as properties coupled to the fractures, e.g. transmissivity.

In this study, 30 Monte Carlo realizations of a synthetic rock mass fracture network are used to study the impact that negligence of the orientation uncertainty has on the connectivity of fracture networks.

The study begins with a brief summary of the findings about the magnitudes of uncertainties during the site investigations performed by the Swedish Nuclear Fuel and Waste Management Co. (SKB). Thereafter a synthetic rock mass fracture network model is created and probed by steep boreholes. The orientations of the intersecting fractures are then altered to reflect what would have been measured in a real world borehole, followed by the development of the orientation model using these altered orientation values. To the last, the connectivity of the fractures in the synthetic rock mass fracture model, i.e. the true fracture network in the rock mass, is compared to the connectivity of the fracture network relying on the altered orientations, i.e. what would be used if measured fracture orientations are used without compensating for the uncertainty.

2. UNCERTAINTIES STEMMING FROM BOREHOLE MEASUREMENTS

During the site investigations performed by SKB, more than 70 boreholes, with a maximum depth of 1 km, were drilled in crystalline rock with a cumulative length of more than 34 km including almost 200,000 single fracture intercepts (SKB, 2008, 2009). These data were used by Stigsson, 2016, to infer the uncertainty distribution for each fracture. In this study seven uncertainties described in Stigsson, 2016, are regarded: borehole diameter variation; measurement of bearing and inclination of the borehole; manual adjustment of the borehole TV image, mapping of intercept angles α and β; and the effect of natural fracture undulation. Each contribution is shortly described below.

The borehole diameter is not constant, but varies slightly along the course of the borehole. Assuming a constant borehole diameter, the uncertainty in geometry will affect the calculation of the α angle. This uncertainty is expressed in Stigsson, 2016, as

$$\sigma_\alpha = 0.4 \cdot \sin(2\alpha_T) \tag{1}$$

Where α_T is the theoretical (measured) angle.

When measuring the orientation of the borehole there are several uncertainties to regard; the inherent uncertainty of the tool; the alignment of the tool to the borehole walls; and the handling of the tool. Stigsson, 2016, inferred the aggregated standard deviation of these uncertainties as

$$\sigma_{incl} = 0.05 + \frac{0.0003}{\cos(incl)}$$
$$\sigma_{bear} = 0.2 + \frac{0.1}{\cos(incl)} \tag{2}$$

Where *incl* is the inclination of the borehole, defined as the angle from the horizontal plane to the local trajectory of the borehole. Observe that a downward pointing borehole has negative inclination.

During the site investigations the orientation of the borehole TV image had to be manually adjusted by a geologist. According to Stigsson, 2016, the contribution to the uncertainty from this manual work is described by

$$\sigma_\beta = 2 - 0.04 \cdot incl \tag{3}$$

The fracture intercepts were mapped using borehole TV when possible. In the case that the trace of the intercept was impossible to detect in the borehole TV image, the orientation was mapped directly on the core, introducing a larger uncertainty. The uncertainties stemming from the mapping is described in Stigsson, 2016, by

$$\sigma_\alpha = \begin{cases} VIB & 1.2 + 0.055 \cdot \alpha \\ notVIB & 1.9 + 0.11 \cdot \alpha \end{cases}$$

$$\sigma_\beta = \begin{cases} VIB & \min\left(\dfrac{9 - 0.06 \cdot \alpha}{\cos(\alpha)} \; ; \; 180\right) \\ notVIB & \min\left(\dfrac{32 - 0.3 \cdot \alpha}{\cos(\alpha)} \; ; \; 180\right) \end{cases} \tag{4}$$

Where *VIB* and *notVIB* refers to the possibility to detect the trace of the fracture intercept in the borehole TV image, or not.

The intercept between the borehole and the fracture only captures the very local orientation of the fracture surface, leaving the general orientation of the fracture unknown. However, assuming that fractures are mono-fractal self-affine surfaces (Mandelbrot, 1985, Russ, 1994, Renard et al., 2006, Candela et al., 2009, Brodsky et al., 2011, and Candela et al., 2012), the uncertainty can be inferred (Stigsson 2016). According to Stigsson, 2016, the standard deviation of the measured fracture orientation is

$$\sigma_\alpha = \arctan\left(\sigma\delta h_{(\Delta L)} \cdot \left(\frac{\phi_{BH}}{\sin(\alpha)}\right)^{(1-D_{Line})}\right)$$

$$\sigma_\beta = \arctan\left(\sigma\delta h_{(\Delta L)} \cdot \phi_{BH}^{(1-D_{Line})}\right) \tag{5}$$

Where $\sigma\delta h_{(\Delta L)}$ is the standard deviation of asperity differences of points ΔL apart; ϕ_{BH} the diameter of the borehole; α the acute angle between the borehole trajectory and the fracture surface; and D_{Line} is the fractal dimension of a trace across the fracture surface.

3. DEVELOPMENT OF MODELS

3.1. Input to Uncertainty Calculations

The findings in sec 2 are used in this study. This implies that a synthetic rock mass similar to the rock masses at the sites where SKB has carried out site investigations (SKB 2008, 2009) is presumed, together with the presumption that the synthetic rock mass is, numerically, probed using similar tools as SKB during the site investigations (SKB 2008, 2009). Other rock types and methods may result in other estimates of uncertainties. The inferred uncertainties, eq (1) to eq (5) are, hence, used to calculate the orientations that would have been achieved during a real site investigation of the synthetic rock mass fracture network. The synthetic rock mass fracture network is probed using steeply inclined boreholes, -80°, with a theoretical diameter of 76 mm. 35% of the fractures are not visible in the borehole TV (SKB 2008, 2009) and, hence, are subjected to larger uncertainties, eq (4). About 50% of the fractures intersecting the drill cores were characterised as slickensided, smooth or rough. A vast majority of these fractures, >90%, were judged to be rough. These fractures are assumed to have $D_{Line} \approx 1.15$, and $\sigma\delta h_{(1mm)} \approx 0.2$ (Stigsson, 2015, and Stigsson and Mas Ivars, 2018). Applicable to >90% of the interpreted fracture surface characteristics, these values are presumed valid for all fractures in the synthetic rock mass fracture network model.

3.2. Input to the Rock Mass Fracture Orientation Model

A rock mass of sparsely distributed water conductive fractures is constructed using the parameters in Table 1. These parameters reflect an idealised rock mass that is inspired by the rock mass in Forsmark (Follin et al., 2007). The model consists of four steeply dipping fracture sets, 45º apart, and one horizontal set. All sets have the same high Fisher concentration parameter, κ, and size location parameter, r_0. The different values of the size shape parameter, k_r, makes the relative fracture intensity, P_{32} (Dershowitz and Herda, 1992), change using different size intervals. For example will the NW and EW set produce very few fractures with radius larger than 5 m, implying that for large fractures the rock mass will consist almost only of NS, NE and SH oriented fractures. Fig 1 shows an equal area plot of this orientation model. This will be referred to as the "rock mass fracture model", i.e. the true distribution of fractures in the rock mass.

Table 1. Indata to the synthetic rock mass fracture network model

Fracture set	NS	NE	NW	EW	SH
Univariate Fisher Orientation Distribution[*]					
Trend (º)	90	135	45	0	0
Plunge (º)	0	0	0	0	90
κ (-)	40	40	40	40	40
Pareto Size Distribution[**]					
r_0 (m)	0.038	0.038	0.038	0.038	0.038
r_{min} (m)	5	5	5	5	5
r_{max} (m)	250	250	250	250	250
k_r (-)	2.5	2.7	3.1	3.1	2.4
Intensities[***]					
$P_{32,r0-564}$ (m^{-1})	0.142	0.345	0.133	0.081	0.316
$P_{32,rmin-rmax}$ (m^{-1})	0.0107	0.0107	0.0006	0.0004	0.0362

[*]Fisher, 1925, [**]Forbes et al. 2011, [***]Dershowitz, 1984

3.3. Calculation of "Measured" Fracture Orientations

The orientation of a fracture measured in a borehole can be calculated using four angles; the bearing and inclination of the borehole together with two angles of the intercept in the local borehole coordinate system, α and β (Stigsson and Munier, 2013). These angles are used to calculate the orientation of the fracture in the global coordinate system using

$$\mathbf{n}_G = \mathbf{Z}_{rot} \cdot \mathbf{Y}_{rot} \cdot \mathbf{n}_{BH} \qquad (6)$$

Where $\mathbf{n}$ denotes the fracture pole vector in global, G, and local borehole, BH, coordinate system respectively; and $\mathbf{Y}_{rot}$ and $\mathbf{Z}_{rot}$ are two rotation matrices.
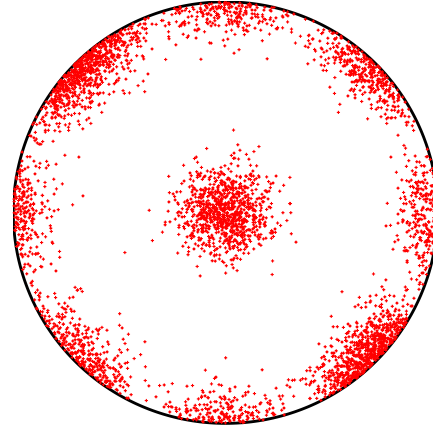

Fig. 1. Equal area projection of the fracture poles from a DFN using parameters from fracture model described in Table 1.

Using the measured values of the four angles, $\mathbf{n}_G$ will reflect the expected orientation of the fracture. However, knowing the uncertainties, the standard deviations of the angles can be calculated according to eq (1) to (5) and, hence, the confidence of the fracture orientation can be inferred. In this case $\mathbf{n}_G$ will be a confidence surface on the stereonet (Stigsson, 2016).

The knowledge of the uncertainties may also be used in a synthetic rock mass fracture network model to estimate what should have been measured in an equivalent real borehole penetrating the fractured rock mass. These stochastically calculated orientations will be referred as "measured" fracture orientations from here on in this study, i.e. what would be recorded mapping a drill core.

The synthetic rock mass fracture network, described in Table 1, was probed by steep boreholes with inclination -80º, and the "measured" fracture orientations were calculated using eq (1) to (6). One outcome of the orientation distribution is visualised in Fig 2.
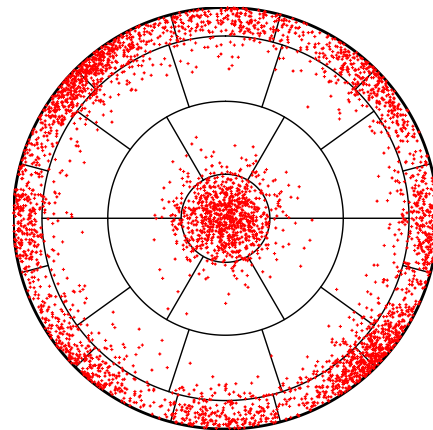

Fig. 2. Equal area projection of the "measured" fracture poles together with the 23 subareas used for the χ^2 tests.

3.4. Orientation analysis

The "measured" fracture orientations were analysed using the FracMan® (Golder Associates, 2014) module ISIS (Interactive Set Identification System) to infer the fracture orientation parameters of the synthetic rock mass, neglecting uncertainty. This reflects what usually is inferred when evaluating orientations. The results from the analysis are shown in Table 2. Comparing the parameters generating the synthetic rock mass fractures, Table 1, with the parameters of the ISIS-analysis shows that there is almost no difference in mean pole trend and plunge between the two sets of parameters. This is in accordance to the findings in Stigsson, 2016. However, for the vertical sets, the Fisher concentration parameter has decreased to about one fourth of the original value and the elliptical Fisher distribution shows a better fit than the univariate Fisher, which is also in accordance to findings in Stigsson, 2016. The parameters for the sub-horizontal, SH, set are only slightly affected due to the boreholes being steeply inclined. A visualisation of the fracture poles of a DFN model using parameters according to Table 2 is shown in Fig 3.

Table 2. Results from the set identification algorithm analysis

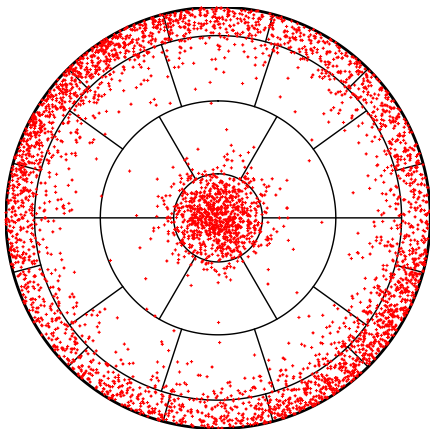| Fracture set	NS	NE	NW	EW	SH
Elliptical Fisher Orientation Distribution[*]					
Trend (º)	91.2	135.7	225.8	359.2	162.4
Plunge (º)	0.7	0.2	0.2	0.6	89.9
Major axis Tr	181.2	45.7	315.8	269.2	276.6
Major axis Pl	1.5	0.9	0.8	3.4	0.0
$\kappa 1$ (-)	11.8	12.0	11.0	12.1	35
$\kappa 2$ (-)	2.1	2.1	2.2	2.2	1
Statistics					
Kolmogorov-Smirnov	0.124	0.107	0.112	0.129	0.02
K-S prob (%)	3.28	5.13	5.15	2.74	100

[*]Golder Associates, 2014

Fig. 3. Equal area projection of fracture poles from a DFN model using data from the ISIS analysis, listed in Table 2.

However, despite that the elliptical Fisher distribution being the best orientation model describing the orientations the fit is poor, cf. the statistics at the two last rows in Table 2, for all but the SH set which have a perfect fit. The poor fits for the four steep sets are mainly due to the fractures modelled as not visible in the borehole TV making the tails long compared to the peaks.

By dividing the stereonet into 23 roughly equally large subareas, Fig 2 to Fig 4, a chi-square, χ^2, test of the orientation distribution can be implemented. This test has the null-hypothesis that the proportions of number of fracture poles in each subarea are statistically equal. Hence, a model using data from Table 2 is generated, probed and the orientations tested against the "measured" poles, Fig 2. The test shows that the null-hypothesis of equal distribution of poles can be rejected on $p = 2.7 \cdot 10^{-4}$, i.e. the models are different with a very high level of confidence.

By changing the orientation parameters manually, a better fit is achieved after a few iterations. The fit is not a perfect, one to one, match, but the match is so good that that the statistical measures can not reject the null-hypothesis of equal distributions, $p = 0.33$. The orientations of the poles from the iterated model are shown in Fig 4. Note that the test *only* can tell that the hypothesis can't be rejected, not that that the models actually are equal. Nevertheless, the iterated model, described in Table 3, is judged to be sufficiently close to be a representative model for the "measured" fracture orientations to be used in the connectivity analyses in this study.
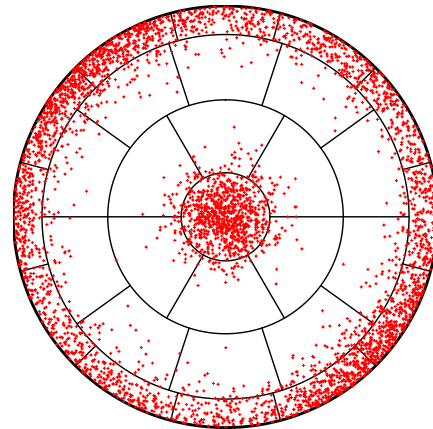

Fig. 4. Equal area projection of fracture poles from a DFN model using the iterated data, listed in Table 3.

The main difference between the orientation parameters from the iterated model, Table 3, and the orientation parameters from the ISIS analysis, Table 2, is that the fracture sets in the iterated model have higher concentration parameter, $\kappa 1$, but lower aspect ratio, $\kappa 2$. This implies that the iterated model has more

concentrated and round fracture sets. A possible explanation why this model works better is that the long tails are hidden within neighboring sets. Hence, the ISIS analysis is more correct on a set by set comparison whilst the iterated model fulfils the global statistic better. Nevertheless, the iterated model is used in the connectivity analysis since it is more conservative making the differences between the synthetic rock mass fracture network and the "measured" fracture network smaller.

Table 3. Parameters from the iterated model, i.e. the parameters that represents what would have been inferred using "measured" fracture orientations neglecting uncertainty.

Fracture set	NS	NE	NW	EW	SH
Elliptical Fisher Orientation Distribution[*]					
Trend (º)	90	135	45	0	0
Plunge (º)	0	0	0	0	90
Major axis Tr	0	45	315	270	0
Major axis Pl	0	0	0	0	0
$\kappa 1$ (-)	28	20	20	20	34
$\kappa 2$ (-)	1.5	1.7	1.7	1.7	1
Pareto Size Distribution[**]					
r_0 (m)	0.038	0.038	0.038	0.038	0.038
r_{min} (m)	5	5	5	5	5
r_{max} (m)	250	250	250	250	250
k_r (-)	2.5	2.7	3.1	3.1	2.4
Intensities[***]					
$P_{32,r0\text{-}564}$ (m^{-1})	0.142	0.345	0.133	0.081	0.316
$P_{32,rmin\text{-}rmax}$ (m^{-1})	0.0107	0.0107	0.0006	0.0004	0.0362

[*]Golder Associates, 2014, [**]Forbes et al. 2011, [***]Dershowitz, 1984

4. CONNECTIVITY ANALYSIS

The fractures in the synthetic rock mass follow the distributions listed in Table 1, which represents the true fractures in the rock mass. In Table 3 are the distribution parameters listed that come from the "measured" fracture orientations and, hence, represent the orientation model that would have been developed, neglecting the uncertainties stemming from the borehole investigations. These two models are used to investigate how the connectivity of a Discrete Fracture Network, DFN (Dershowitz, 1984, and references therein), is affected if the orientation uncertainty is neglected when developing DFN's from fracture intercepts in steeply inclined boreholes.

The connectivity analysis is carried out in 30 cubes of 1 km^3 each, containing fractures in the size range 5 to 250 m radius. In the center of the cube, a 50 m long horizontal line, trending East-West, is inserted. This line acts as the starting boundary for the connected fracture

network, and the growth is studied for each level of connection. I.e. the first level includes the fractures intersecting the horizontal line; the second level includes the fractures that intersect the fractures that interest the line etc. Due to the sparseness of the DFN about 1/3 of the realization do not yield any connection between the horizontal line and the borders of the 1 km^3 cube. For the remaining 2/3, four to nine levels of connections are needed until the first fracture hits any border of the cube.

To eliminate impacts from different spatial locations of the fractures the same seed is used for the two models. This implies that only the orientation will differ between the same fractures in the two models, i.e. the number of fractures, the locations and the sizes are all equal, Fig 5.
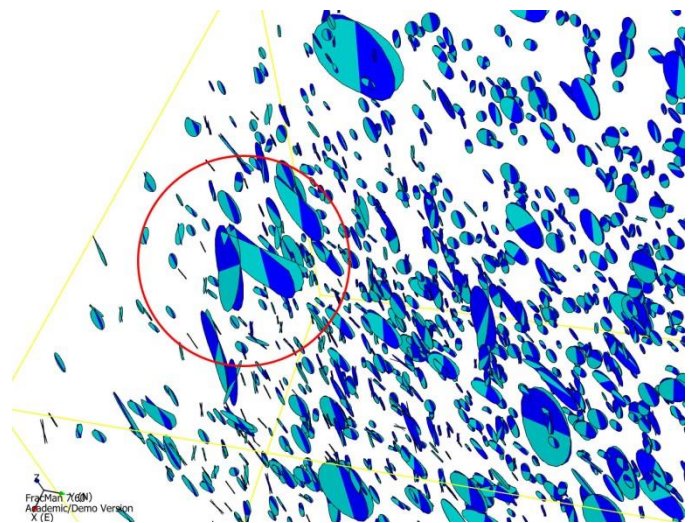

Fig. 5. The differences in orientation between the two models, rock mass fracture model fractures (blue) and "measured" fracture model fractures (turquoise), for the NE set. The red circle highlights an example of two fractures connected in the "measured" fracture orientation model that is not connected in the rock mass fracture model.

The difference of the different fracture network pairs can be qualitatively evaluated by visual inspection. Fig 6 and Fig 7 shows the evolution of two realisations, R1 and R2, at different connectivity levels. The networks are visualised looking from North to South due to the NS, and SH sets being the most dominant sets.

During the first few connectivity levels, usually 1 to 4, there are almost no visual differences between the two DFN's, but as the networks grow the differences increase until the networks hits the borders. After that, adding new connectivity levels will only fill the cube with fractures making it difficult to see any differences.
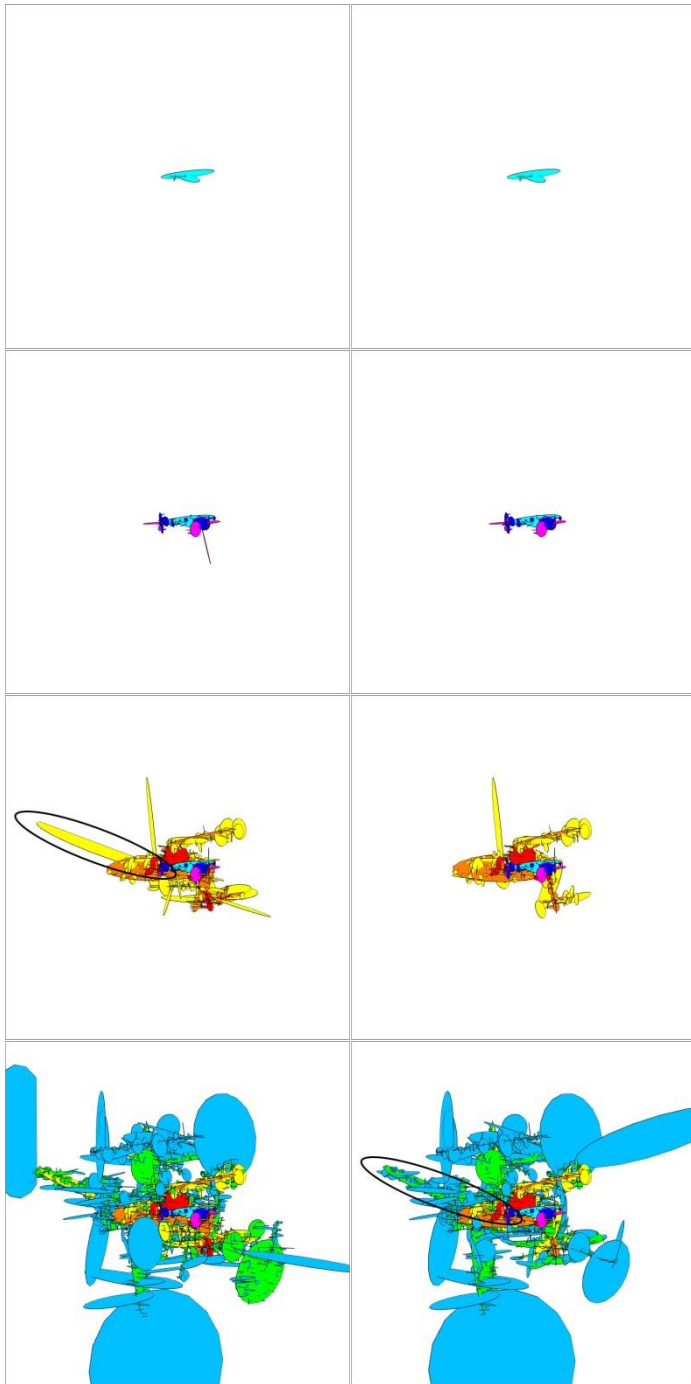
Fig. 6. The evolution of the extension of a connected fracture network, R1. To the left, the rock mass fracture model and to the right, the "measured" fracture model. From top row to bottom; North view of level 1, level 3, level 6 and level 8. Specially note that the "measured" fracture orientation model lacks connection to a large fracture at level 6, (marked with a black ellipse in the rock mass fracture model, left column) but it is connected at higher levels (marked with a black ellipse, right column) in the "measured" fracture model.

The orientations of the fractures in the rock mass fracture model are less spread from the mean pole of each set, than the fractures in the "measured" fracture orientation model. Hence, in the rock mass fracture model the fractures reach slightly further out in space perpendicular to the directions of the fracture sets' mean poles. This has the effect that the rock mass fracture

model usually grows faster than the "measured" fracture orientation model in these directions. In contrary, the fractures in the "measured" fracture model have a higher probability to intersect other fractures that are located parallel to the fracture sets' mean poles, as highlighted in Fig 5.
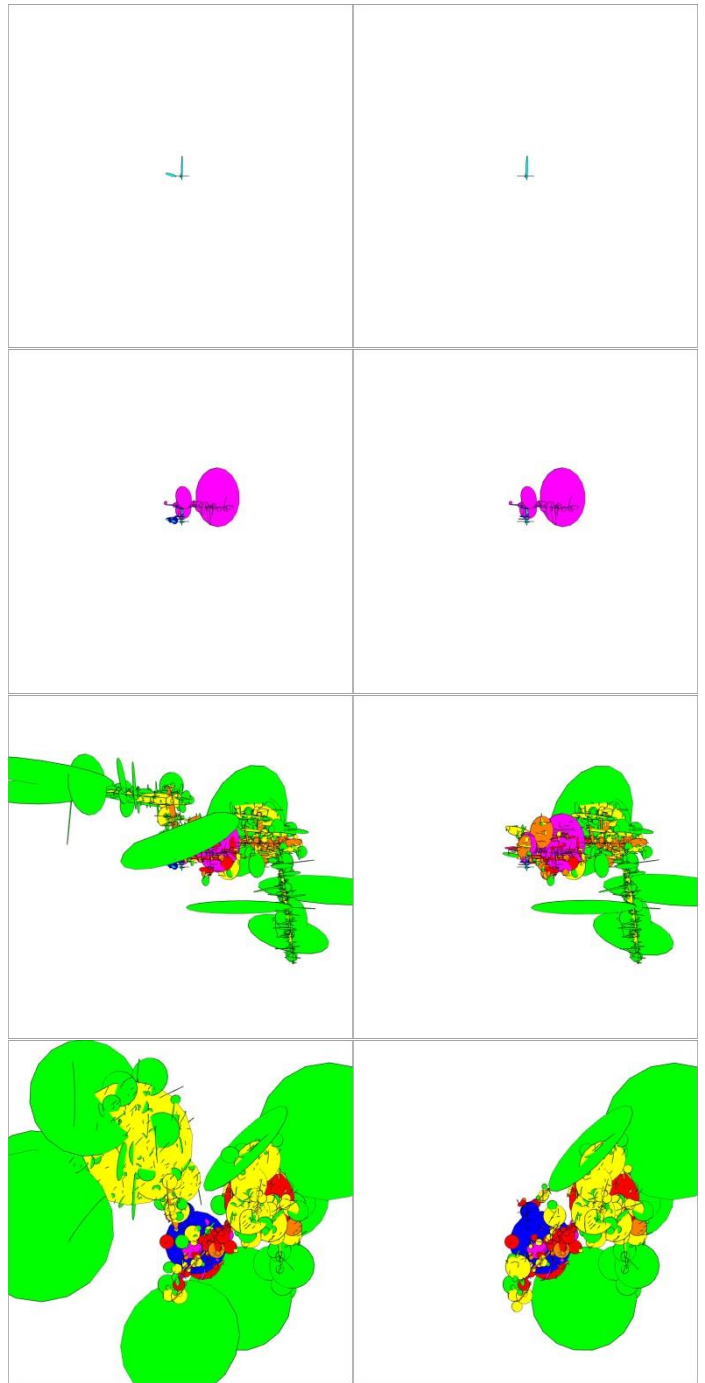

Fig. 7. The evolution of the extension of a connected fracture network, R2. To the left, the rock mass fracture model and to the right, the "measured" fracture model. From top row to bottom; North view of level 1, level 3, level 7 and top view of level 7.

In the case that two larger fractures are connected in the rock mass fracture model, but not in the "measured" fracture model, they will often be connected in the next connectivity level in the "measured" fracture model.

This implies that there often are small fractures in-between the two large fractures bottlenecking the system. An example of this is seen in Fig 6 where the large yellow fracture to the left in the rock mass fracture model at level 6 is absent in the "measured" fracture model at level 6, but is seen as a green fracture in the "measured" fracture orientation model at level 8.

In some realisations the connectivity between large fractures remains absent. This has the effect that the connectivity becomes very different between the rock mass fracture model and "measured" fracture model. An example of this is seen in Fig 7 where a large part of the fracture cluster is absent in the "measured" fracture model at level 7. The network is shown both from North and from the top to highlight the large difference.

The number of fractures making up the connected network is roughly equal for the first few connectivity levels, 1 to 3, for a unique model comparison, i.e. two models using same seed. At the connectivity level where the first fracture intersects a border of the cube, usually level 5 to 9, the rock mass fracture model usually have about 30% more fractures attached to the cluster compared to the "measured" fracture model. The size distributions of the connected fractures are about equal for the two models. Hence, a 30% increase in number of fracture results in a 60-70% increase in connected area.

The elongation of the fracture clusters is estimated using the ratio between the equivalent radius, using the volume of the convex hull of the cluster, and the equivalent radius, using the surface area of the convex hull of the cluster. For a sphere this ratio will be 1, and the more elongated the larger ratio. This measure does not infer the direction of the elongation but rather the ratio between the largest and smallest axes. This ratio is between 1.1 and 1.15 for the rock mass fracture models when the first connected fracture hits the boundary of the 1 km^3 cube. These values correspond to an aspect ratio of about 4:1 between the major and minor axis of an idealised lens. For the "measured" fracture orientation models the corresponding ratio is between 1.05 and 1.1 corresponding to an aspect ratio of about 3:1 between the major and minor axis. Hence, the rock mass fracture model results in slightly more elongated fracture clusters than the clusters of the "measured" fracture model.

5. DISCUSSION

The DFN used to represent the "measured" fracture model has most certainly overestimated concentration parameters of the orientation distribution. This implies that the differences in connectivity between the rock mass fracture model and the "measured" fracture model are underestimated. Using another model, such as the set by set analysis using ISIS module in FracMan®, would result in larger differences in the spatial extension of the DFN's. Despite the under estimation of orientation differences, there are still both qualitative and quantitative differences in the extensions of the connected fracture networks.

Most often the same fractures are connected, especially for the cases where the boundary is reached using few connectivity levels, about 4 to 6 levels. For the cases where more levels are needed, the "measured" fracture orientation models more often need small fractures to bring gaps between larger fractures. This implies that the fracture network using "measured" fracture orientations more often have bottlenecks affecting, e.g. flow and transport of solutes, compared to the rock mass fracture model.

The clusters in the rock mass fracture models have about 60% more fracture area than the corresponding "measured" fracture orientation models. This might imply faster pathways for particles in the rock mass fracture models.

Also the difference in elongation of the clusters, 4:1 for the rock mass fracture model and 3:1 for the "measured" fracture model, indicates more preferential flow directions for the rock mass model, i.e. the real rock, than the "measured" fracture model, i.e. the model neglecting orientation uncertainty when developing the orientation model.

It is, however, noticed that for the current set up of parameters, a sparsely fractured rock mass, the difference between realizations will probably have larger effect than the uncertainty of the orientation parameters. If this is the case for model setups using for example larger differences in concentration parameters for the orientation distribution or higher fracture density still needs to be investigated.

It is also noted that the results comes from a limited number of realizations, 30, and hence it can not be stated with any significance that the differences seen in this study is systematical. A more systematic set up, varying the parameters size, intensity and orientation, together with many, >100, Monte Carlo realizations for each parameter combination could bring more light to parameter combinations where the orientation uncertainty is severely affecting the connectivity of DFN's.

6. CONCLUSIONS

The study has shown that it is possible to infer the parameters to describe the fracture network in the rock mass knowing the measured orientation together with the uncertainty for each fracture intercept. Neglecting this knowledge of uncertainty the orientation model will be erroneous, and this error will affect the connectivity of the DFN.

The rock mass fracture model, i.e. the true rock, usually have 30% more connected fractures and 60% more connected fracture area than the "measured" fracture model, i.e. the model ignoring uncertainty information, at the connectivity level where the first fracture of the clusters hits any boundary of the 1 km^3 cube. The rock mass fracture model is also more elongated than the "measured" fracture model. Hence, the connectivity differs between the fracture model based on "measured" fracture orientations and the model based on the rock mass fracture orientations.

This study only cover one setup of parameters and rely on too few realisations to put any significance on the differences seen, i.e. if there is a systematic bias between the true rock and the model ignoring uncertainty. The study however shows that there are differences in connectivity between the two fracture networks.

Thus, in short, if you did forget the measurement uncertainties, the connectivity in your DFN model is specious!

ACKNOWLEDGEMENT

REFERENCES

1. Brodsky E., J. Gilchrist, A. Sagy and C. Collettini. 2011. Faults smooth gradually as a function of slip. *Earth and Planetary Science Letters* 302 (2011) 185–193

2. Candela T, F. Renard, M. Bouchon, D. Marsan, J. Schmittbuhl and C. Voisin. 2009. Characterization of Fault Roughness at Various Scales: Implications of Three-Dimensional High Resolution Topography Measurements. In: *Mechanics, Structure and Evolution of Fault Zones*, eds Y. Ben-Zion and C. Sammis. Birkhäuser Basel

3. Candela T., F. Renard, Y. Klinger, K. Mair, J. Schmittbuhl and E. Brodsky. 2012. Roughness of fault surfaces over nine decades of length scales. *Journal of Geophysical Research*, vol. 117, B08409, doi:10.1029/2011JB009041

4. Dershowitz W. S. 1984. Rock joint systems. PhD thesis, Massachusetts Institute of Technology, Boston, USA, 1984

5. Dershowitz W. S. and H. Herda. 1992. Interpretation of fracture spacing and intensity. In: *Proc., 33rd U.S. Symp. on Rock Mechanics, Santa Fe, New Mexico 757–766*. Rotterdam: Balkema

6. Fisher R. A. 1925. *Statistical methods for research workers*. Genesis Publishing Pvt Ltd. ISBN 8130701332.

7. Follin S., J. Levén, L. Hartley, P. Jackson, S. Joyce, D. Roberts and B. Swift. 2007. Hydrogeological characterisation and modelling of deformation zones and fracture domains, Forsmark modelling stage 2.2. Updated 2013-12. Swedish Nuclear Waste Management Co. available at: https://www.skb.se/publikation/1540554/R-07-48.pdf

8. Forbes C., M. Evans, N. Hastings and B. Peacock. 2011. *Statistical istributions. 4th edition*. John Wiley & Sons Inc. ISBN 978-0-470-39063-4

9. Golder Associates Inc. 2014. FracMan® Discrete Fracture Network Modelling Software, User Documentation, Nuclear Edition, Version 7.4., Golder Associates Inc, Redmond, 2014.

10. Mandelbrot B. B. 1985. Self-Affine Fractals and Fractal Dimension. Physica Scripta. Vol. 32, 257-260, 1985.

11. Renard F., C. Voisin, D. Marsan and J. Schmitbuhl. 2006. High resolution 3D laser scanner measurements of a strike-slip fault quantify its morphological anisotropy at all scales, *Geophys. Res. Lett.* 33, L04305, doi: 10.1029/2005GL025038

12. Russ J. 1994. *Fractal Surfaces*. Plenum Press, New York. ISBN 0-306-44702-9

13. SKB. 2008. Site description of Forsmark at completion of the site investigation phase. SDM-Site Forsmark. SKB TR-08-05. Swedish Nuclear Waste Management Co. available at: http://www.skb.se/upload/publications/pdf/TR-08-05.pdf.

14. SKB. 2009. Site description of Laxemar at completion of the site investigation phase. SDM-Site Laxemar. SKB TR-09-01. Swedish Nuclear Waste Management Co. available at: http://www.skb.se/upload/publications/pdf/TR-09-01.pdf.

15. Stigsson M. 2015. Parameterization of fractures - Methods and evaluation of fractal fracture surfaces. TR 15-27. POSIVA OY. Available at: http://www.posiva.fi/en/databank/workreports?xm_freetext=stiggson

16. Stigsson M. 2016. Orientation Uncertainty of Structures Measured in Cored Boreholes: Methodology and Case Study of Swedish Crystalline Rock. Rock Mech Rock Eng (2016) 49: 4273. https://doi.org/10.1007/s00603-016-1038-5

17. Stigsson M. and D. Mas Ivars. 2018. A novel conceptual approach to objectively determine JRC using fractal dimension and asperity distribution of mapped fracture traces, *in progress*.

18. Stigsson M, and R. Munier. 2013. Orientation uncertainty goes bananas: An algorithm to visualise the uncertainty sample space on stereonets for oriented objects measured in boreholes. Computers & Geosciences, vol 56, july 2013, pp56-61. http://dx.doi.org/10.1016/j.cageo.2013.03.001